Assessing agricultural drought in summer over Oklahoma Mesonet sites using the water-related vegetation index from MODIS

Rajen Bajgain[1], Xiangming Xiao[1,2], Jeffrey Basara[3,4], Pradeep Wagle[1], Yuting Zhou[1], Yao Zhang[1], Hayden Mahan[3]

[1] Department of Microbiology and Plant Biology, Center for Spatial Analysis, University of Oklahoma, 101 David L. Boren Blvd, Norman, OK 73019, USA [2] Ministry of Education Key Laboratory for Biodiversity Science, and Engineering, Institute of Biodiversity of Sciences, Fudan University, Shanghai 200433, China [3] School of Meteorology, University of Oklahoma, Norman, OK, USA [4] Oklahoma Climate Survey, Norman, OK, USA

Abstract

Agricultural drought, a common phenomenon in most parts of the world, is one of the most challenging natural hazards to monitor effectively. Land surface water index (LSWI), calculated as a normalized ratio between near infrared (NIR) and short-wave infrared (SWIR), is sensitive to vegetation and soil water content. This study examined the potential of a LSWI-based, drought-monitoring algorithm to assess summer drought over 113 Oklahoma Mesonet stations comprising various land cover and soil types in Oklahoma. Drought duration in a year was determined by the number of days with LSWI <0 (DNLSWI) during summer months (June–August). Summer rainfall anomalies and LSWI anomalies followed a similar seasonal dynamics and showed strong correlations (r^2 = 0.62–0.73) during drought years (2001, 2006, 2011, and 2012). The DNLSWI tracked the east-west gradient of summer rainfall in Oklahoma. Drought intensity increased with increasing duration of DNLSWI, and the intensity increased rapidly when DNLSWI was more than 48 days. The comparison between LSWI and the US Drought Monitor (USDM) showed a strong linear negative relationship; i.e., higher drought intensity tends to have lower LSWI values and vice versa. However, the agreement between LSWI-based algorithm and USDM indicators varied substantially from 32 % (D_2 class, moderate drought) to 77 % (0 and D_0 class, no drought) for different drought intensity classes and varied from ~30 % (western Oklahoma) to >80 % (eastern Oklahoma) across regions. Our results illustrated that drought intensity thresholds can be established by counting DNLSWI (in days) and used as a simple complementary tool in several drought applications for semi-arid and semi-humid regions of Oklahoma. However, larger discrepancies between USDM and the LSWI-based algorithm in arid regions of western Oklahoma suggest the requirement of further adjustment in the algorithm for its application in arid regions.

Keywords: Drought duration, Drought intensity, Land surface water index, Summer drought

Introduction

Drought is a recurrent and inevitable threat in several parts of the world (Hulse and Escott 1986; Shahid and Behrawan 2008; Sönmez et al. 2005). Southern Great Plains of the USA experience drought on varying spatial and temporal scales (Basara et al. 2013; Christian et al. 2015). Drought is also among the most difficult of all natural hazards to monitor effectively.

Yet, the repeated occurrence of drought events has highlighted the need to develop effective drought-monitoring tools to assess the impacts of this phenomenon. Research to retrieve leaf water content from the reflectance acquired from satellite sensors has progressed for more than three decades. Tucker 1980 first suggested that the 1550–1750-nm spectral intervals were the best-suited band in the 700–2500-nm region for monitoring plant canopy water status from space. A number of broadband ratio and combination techniques using Thematic Mapper (TM) channel 4 (760–900 nm, near infrared) and TM channel 5 (1550–1750 nm, shortwave infrared) were proposed for remote sensing of plant water status (Hunt et al. 1987; Jackson et al. 1983). The combination of the near infrared (NIR) and short-wave infrared (SWIR) bands has the potential of retrieving vegetation canopy water content (Ceccato et al. 2001, 2002; Maki et al. 2004). The water-related vegetation index computed from the combination of NIR and SWIR has different nomenclatures by different authors. Gao 1996 and Chen et al. 2005 referred it the normalized difference water index (NDWI). Kimes et al. 1981 used the term normalized difference infrared index (NDII). Similarly, Jurgens 1997 and Xiao et al. 2002a, b called the same combination of NIR and SWIR bands as the land surface water index (LSWI). Despite known by different names, the features they have in common is that the NIR spectral region serves as a moisture reference band and the SWIR spectral domain is used as the moisture-measuring band. The water-related vegetation index is a measurement of liquid water in vegetation canopies and hence is sensitive to the total amount of liquid water contained in vegetation when the vegetation cover is high. Some recent studies (Bajgain et al. 2015; Chandrasekara et al. 2011; Wagle et al. 2014) have identified LSWI as an index in extracting the vegetation water status and in drought detection.

Because agricultural drought occurs due to lack of soil moisture and the consequent water stress in the vegetation, a water-based index should also be used along with the greenness-related indices such as normalized difference vegetative index (NDVI) and enhanced vegetative index (EVI) to develop systematic and effective method of agriculture drought assessment (Bajgain et al. 2015; Chandrasekara et al. 2011; Tian et al. 2013; Wagle et al. 2014). The Moderate Resolution Imaging Spectrometer (MODIS) sensor on board the NASA Terra satellite platform provides continuous daily observations of the land surface. Our hypothesis is that the water-related vegetation index LSWI computed from time series MODIS images offers a new and improved capacity for drought monitoring. In this study, we evaluated the hypothesis over 113 Mesonet sites across Oklahoma under different land cover and soil types. Also, the drought intensity class classified

based on LSWI values corresponding to US Drought Monitor (USDM) drought intensity classes are further linked to the duration of LSWI <0 (DNLSWI) to establish a certain threshold of DNLSWI (in days) to define drought intensity classes. Therefore, results from this study will help in improving the capability of remote sensing vegetation drought monitoring by establishing LSWI as a complimentary tool to existing NDVI-based drought products. Specifically, we addressed the following research questions:

1. Is LSWI anomaly able to capture the drought events across multiple sites over years?

2. Is LSWI-based drought-monitoring algorithm developed for two tallgrass prairie sites (Bajgain et al. 2015) applicable to quantify drought intensity over 113 Mesonet sites comprising various land cover and soil types in Oklahoma?

3. What is the relationship between the DNLSWI and drought intensity classified by USDM?

Materials and methods

Data

Oklahoma Mesonet stations and rainfall data

An extensive environmental observation network is well established and distributed over Oklahoma, known as the Oklahoma Mesonet (Brock et al. 1995). The Oklahoma Mesonet is a network of 120 automated stations with at least 1 in each 77 counties of Oklahoma. The Mesonet provides quality-controlled measurements of meteorological and land-surface variables such as precipitation, temperature, and soil moisture at intervals spanning 5–30 min depending on the variables (http://www.Mesonet.org/).

In this study, we used 113 Mesonet stations that have continuous measurements of meteorological parameters from 2000 to 2013. Retired and replaced Mesonet stations were not considered because site replacements were on different MODIS pixels. The locations of the selected sites are presented in Fig. 1; biophysical features are presented in Table S1. In this study, we used the precipitation and soil water content (SWC) data for three summer months (June–August) and calculated the rainfall and SWC anomalies from the 14-year mean (2000–2013). Additionally, the anomalies in rainfall calculated from 30-year rainfall data (climatological normal) from Cooperative Observer Program (COOP, National Weather Service) sites were compared with the rainfall anomalies computed from a 14-year data from Mesonet stations, two from each climate division of Oklahoma.

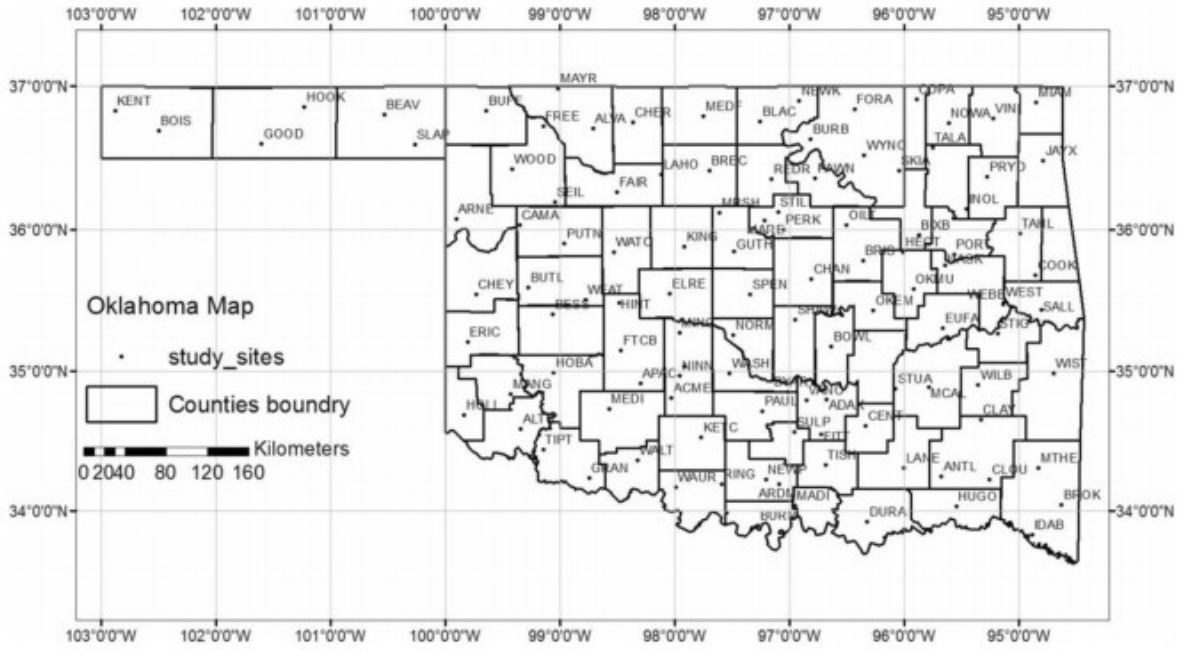

FIGURE 1 The location and distribution of the Mesonet sites (113 Mesonet stations) in Oklahoma, USA

MODIS surface reflectance and vegetation index data

The MODIS is an instrument on board the NASA's Terra (EOS am) and Aqua (EOS pm) spacecraft. This sensor provides simultaneous observations of the atmosphere, terrestrial surface, and oceans. The MODIS instrument has a temporal resolution of 1 to 2 days with high radiometric resolution images (12 bit). It collects data for 36 spectral bands, and the following 7 of these bands are designated mainly for land surface and vegetation studies: blue (459–479 nm), green (545–565 nm), red (620–670 nm), near infrared (nir1 841–875 nm and nir2 1230–1250 nm), and shortwave infrared (swir1 1628–1652 nm and swir2 2105–2155 nm; Lillesand et al. 2014).

The 8-day MODIS land surface reflectance product (MOD09A1) at a 500-m spatial resolution was used in this study. The MOD09A1 time series datasets for individual Mesonet sites were downloaded from the data portal managed by the Earth Observation and Modeling Facility at the University of Oklahoma (http://eomf.ou.edu/visualization). The geographic locations of the Mesonet sites were used to retrieve MODIS data at pixel level. For each MODIS 8-day composite, surface reflectance (ρ) values for visible, NIR, and SWIR bands were used to calculate NDVI, EVI, and LSWI as

$$\mathrm{NDVI} = \frac{\rho\,NIR1 - \rho red}{\rho\,NIR1 + \rho red} \quad (1)$$

$$\mathrm{EVI} = \frac{\rho\,NIR1 - \rho red}{\rho\,NIR1 + 6 \times \rho red - 7.5\,\rho\mathrm{blue} + 1} \quad (2)$$

$$\mathrm{LSWI} = \frac{\rho\,NIR1 - \rho\mathrm{SWIR1}}{\rho\,NIR1 + \rho\mathrm{SWIR1}} \quad (3)$$

USDM data

The USDM map is a weekly drought product developed by a partnership of various agencies including National Oceanic and Atmospheric Administration (NOAA), the US Department of Agriculture (USDA), and the National Drought Mitigation Center (NDMC) (http://www.drought.unl.edu/MonitoringTools/USDroughtMonitor.aspx). The USDM includes a weekly national map displaying dryness divided into five categories, or levels of intensities, from D_0 to D_4, based on a percentile ranking of numerous indicators or indices (Svoboda et al. 2002). The *D* levels are based on a blend of different indices including the Palmer drought index, CPC soil moisture model, US Geological Survey (USGS) weekly streamflow, standardized precipitation index (SPI), and satellite vegetation health index (Kogan 2002; Kogan et al. 2004). The *D* levels are labeled by drought intensity or severity, with D_1 being the least intense and D_4 the most intense. The D_0 classification or drought watch areas are abnormally dry and may be heading into drought or recovering from drought, but conditions have not yet returned to normal (Svoboda et al. 2002). The USDM archived weekly maps are available at http://droughtmonitor.unl.edu/archive.html.

For this study, weekly USDM drought maps for June–August (2000 to 2013) were provided by the NDMC in shapefile format and then rasterized to the 10-km ALEXI CONUS grid. Numerical values were assigned to each drought category, with no drought conditions set to 0, abnormally dry conditions (D_0) to 1, moderate drought (D_1) to 2, severe drought (D_2) to 3, extreme drought (D_3) to 4, and exceptional drought (D_4) to 5.

Methods

LSWI-based agricultural drought-monitoring algorithm

The LSWI-based algorithm uses LSWI as an indicator to assess agricultural drought in tallgrass prairie (Bajgain et al. 2015). Generally, green vegetation has positive LSWI values (>0) and dry vegetation has negative LSWI values (<0). Therefore, LSWI <0 during growing season indicates drought in tallgrass prairie in Oklahoma (Bajgain et al. 2015; Wagle et al. 2014). The duration of LSWI <0 (DNLSWI) during the summer months (June–August) was used to estimate the drought duration and drought intensity. To illustrate the algorithm at single site, the dynamics of rainfall and LSWI in drought (2006) and pluvial year (2007) at Marena Mesonet station is presented in Fig. 2. The LSWI was greater than zero throughout the growing season in 2007 when ecosystem received well-distributed rainfall, while the LSWI was less than zero for substantial number of days in 2006 due to rainfall associated with drought (Dong et al. 2011). Therefore, we used DNLSWI during the summer months (June–August) to reflect the duration (length) of drought period as an algorithm to assess summer drought of the ecosystem.

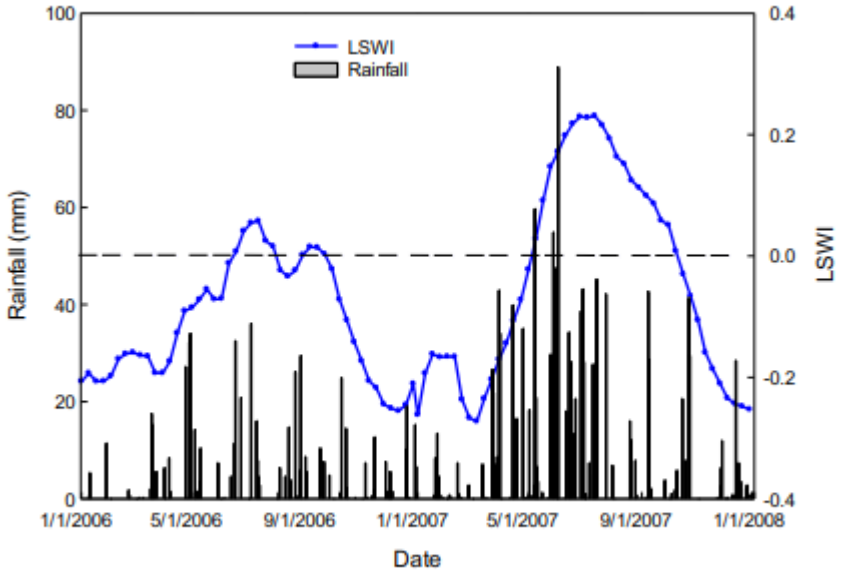

FIGURE 2 Seasonal dynamics and interannual variations of daily rainfall and land surface water index (LSWI) in drought (2006) and pluvial (2007) years at Marena, Oklahoma

Anomaly analysis of summer rainfall and LSWI

Mean LSWI was computed for the summer months, and anomalies were determined for each station during drought years (2001, 2006, 2011, and 2012) from the 14-year mean (2000–2013). Similarly, summer rainfall anomalies were computed for each station during drought years based on the 14-year mean. The similarity between the LSWI anomaly and summer rainfall anomaly for each station was determined by evaluating the correlation between them. This method identified the stations where LSWI anomalies followed the trends of summer rainfall anomalies, thus providing a direct method to assess ecosystem drought.

Results

Characteristics of summer rainfall over 113 Mesonet sites and identification of drought years based on summer rainfall

Figure 3a shows the box plots of the total summer rainfall that occurred in each year over the 113 Mesonet sites. The dispersion in the rainfall among the 113 stations is compared for each year, and the line in the box represents the median summer rainfall amount, which is equivalent to the 50th percentile of observations (113 stations). The median summer rainfall was highest (455 mm) in 2007, while the years including 2001, 2006, 2011, and 2012 had relatively low median rainfall. For example, 50 % of the observations were below 111 mm of summer rainfall in 2011, indicating dry conditions at more than half of the Mesonet stations and was consistent with significant drought during the period (Hoerling et al. 2013; Tadesse et al. 2015).

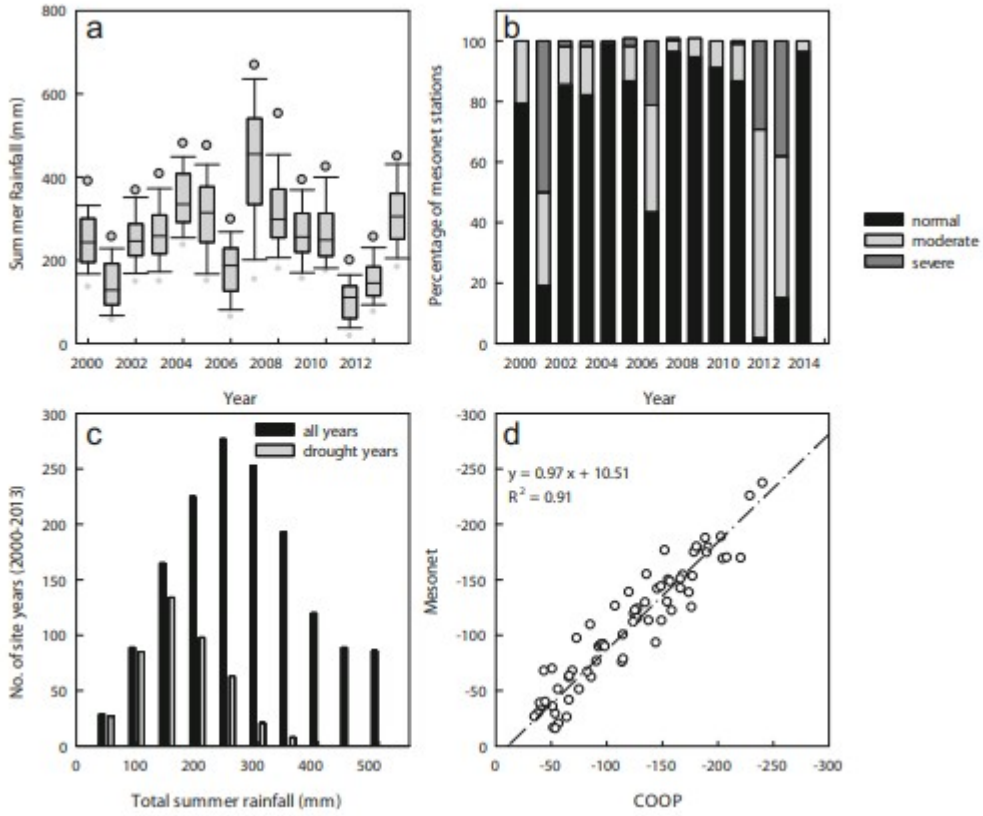

FIGURE 3 Summer rainfall across 113 Mesonet sites during 2000–2013 (**a**). The *solid lines in the box* represent the median, and the *dots above and below the box* represent the 95th and 5th percentiles, respectively. Yearly summer drought analysis by rainfall deficiency: percentage of the Mesonet stations under three drought categories (severe, moderate, and normal) for 2000–2013 (**b**). The frequency distribution of site-year grouped under different summer rainfall regimes (**c**) for whole study period (2000–2013) and for drought years (2001, 2006, 2011, and 2012). Correlation of rainfall anomalies calculated from 30-year rainfall data from Cooperative Observer Program (COOP) and 15-year rainfall data from Mesonet stations (**d**)

The analysis of summer drought for each year (2000–2013) was computed by calculating the average summer rainfall from the14-year average. Precipitation values representing 50 and 25 % of the long-term average rainfall were calculated for each station. These values were then deducted from the long-term average at every station to obtain values of 25 and 50 % precipitation. If the annual rainfall was between 25 and 50 % deficiency, then it was classified as moderate drought. If the annual rainfall was less than the value of 50 % deficiency, then it was classified as severe drought. For example, at the Acme Mesonet station:

$$\text{Average summer rainfall (1981–2010)} = 260 \ mm .$$
$$5050\% \text{of average summer rainfall} = 50\% \text{of } 260 = 130 \ mm.$$
$$25\% \text{of average summer rainfall} = 25\% \text{of } 260 = 65 \ mm .$$
$$50 \ \% \ \text{deficiency} = 260 - - 130 = 130 \ mm .$$
$$25 \ \% \ \text{deficiency} = 260 - - 65 = 195 \ mm .$$
$$\text{Summer rainfall during 2011} = 83 \ mm .$$

Thus, the summer rainfall at Acme in 2011 was less than the calculated 50 % deficiency and was subsequently classified as severe drought.

Based on annual rainfall deficiency, the majority of the stations received less than normal amounts of rainfall in 2001, 2006, 2011, and 2012, whereas stations received normal to above normal rainfall in 2004, 2007, 2008, and 2013 (Fig. 3b). For example, in 2011, drought occurred at nearly all stations, whereby 70 % of stations included at least the moderate drought classification with 29 % of those classified as severe.

A frequency distribution was completed for drought periods when compared with the total period by computing total summer rainfall (June–August) for 1582 site-years (14 years × 113 sites) of total data. The results displayed in Fig. 3c demonstrate that drought site years have a significant right skew in distribution, whereby the summer rainfall ranged from 50 to 350 mm with the greatest number falling within 150-mm bin. Conversely, the frequency distribution for all years (drought plus normal) ranged from 50 to 500 mm with the highest number falling within the 250-mm bin.

Figure 3d shows the anomalies in summer rainfall calculated from a 30-year rainfall data (climatological normal) from COOP sites compared with the rainfall anomalies computed from a 14-year data from Mesonet stations, two from each climate divisions of Oklahoma. The correlation analysis showed a strong relationship ($r^2 = 0.91$) between the anomalies of rainfall obtained from two data sources, suggesting that drought years (2001, 2006, 2011, and 2012) identified in our analysis can represent the climatic extremes of Oklahoma in the last decade based on climatological normal perspective.

The relationship between rainfall anomaly and LSWI anomaly

Once the drought years were selected, the relationship between summer rainfall anomalies and LSWI anomalies was investigated. Figure 4 displays the LSWI anomalies and summer rainfall anomalies for individual pixels over the 113 Mesonet stations during drought years (2001, 2006, 2011, and 2012). Overall, the anomalous summer rainfall results in anomalous LSWI at most Mesonet stations during drought years. As such, the anomalies in summer rainfall and LSWI revealed a strong relationship between rainfall and vegetation water content. For example, pixel-based correlation analyses between summer rainfall anomalies and LSWI anomalies are presented in Fig. 4 (inset graphs). For all identified drought years, strong relationships ($r^2 = 0.61–0.67$) between anomalies of summer rainfall and anomalies of LSWI were identified. Although the magnitudes of the anomalies of summer rainfall and LSWI varied from year to year, the relationship between two parameters was consistently strong.

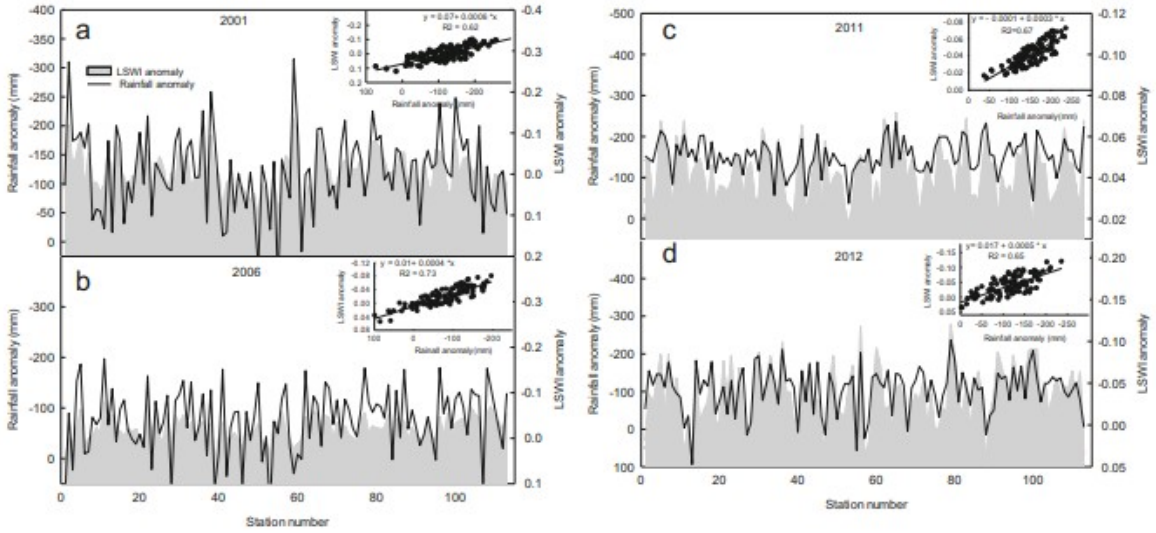

FIGURE 4 Dynamics of summer rainfall and LSWI anomalies in drought years a 2001, b 2006, c 2011, and d 2012 at 113 Mesonet stations. The inset graphs are the regression analyses between summer rainfall and LSWI anomalies (n = 113)

The relationship between SWC anomaly and vegetation indices anomaly

Figure 5 presents the Pearson's correlation coefficients (r) between SWC anomalies and three vegetation anomalies (NDVI, EVI, and LSWI). As expected, a better relationship (r_{LSWI} = 0.52) of SWC anomalies was observed with LSWI anomalies than NDVI anomalies (r_{NDVI} = 0.40) and EVI anomalies (r_{EVI} = 0.44). We examined the correlation coefficients (r_{LSWI}, r_{EVI}, and r_{NDVI}) for all 113 Mesonet stations. Figure 6 compares the r values derived for NDVI, EVI, and LSWI anomalies with SWC anomalies. The analysis showed the significant difference between r_{LSWI} and r_{NDVI} and r_{LSWI} and r_{EVI} with p values less than 0.0001. As a whole, there are significant r values that fall above the 1:1 line towards the r_{LSWI}. The r_{LSWI} was 25 and 20 % higher than r_{NDVI} and r_{EVI}, respectively, suggesting LSWI as a better indicator of soil water content as compared to NDVI and EVI.

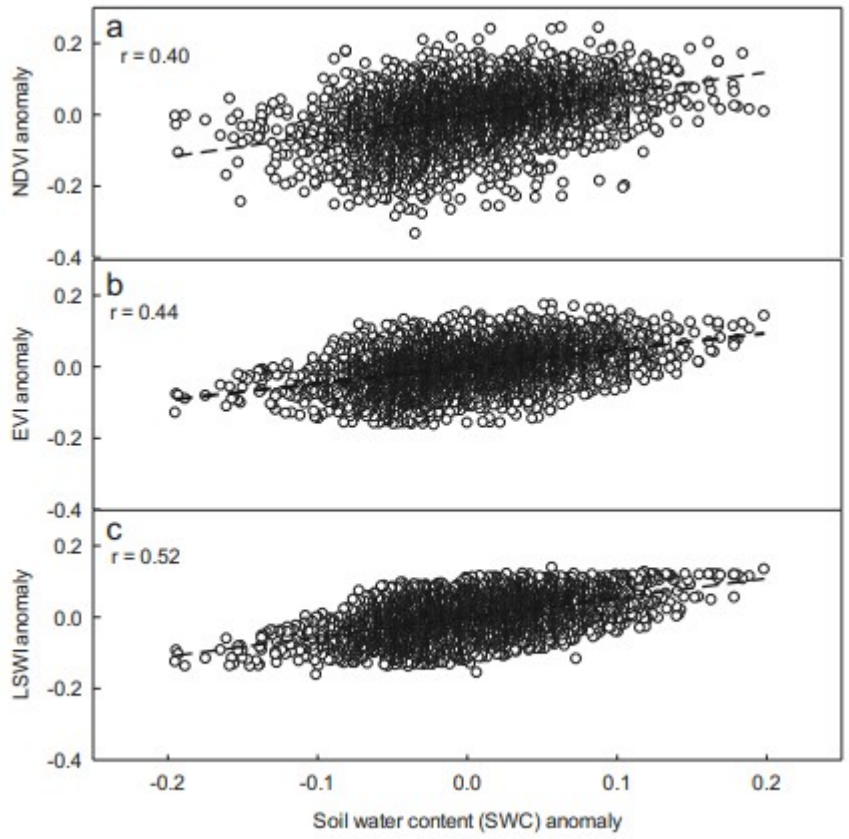

FIGURE 5 Correlation analysis between soil water content (SWC) anomaly and vegetation index (VI) anomalies a NDVI, b EVI, and c LSWI. Each point represents the VI anomalies and SWC anomaly value for each month of the summer from 2000 to 2013

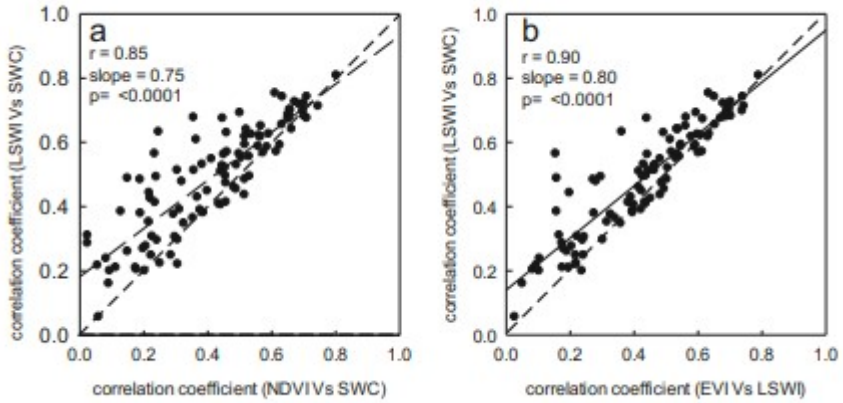

FIGURE 6 Relationship between the 1.0 values of correlation coefficients of VI anomalies and SWC anomaly. Each point represents the correlation coefficient obtained by plotting monthly anomaly values for each station

The relationship between LSWI-based drought duration and summer rainfall

Figure 7 shows the scatter plot of DNLSWI versus total summer rainfall across 113 Mesonet stations binned into 50-mm classes. The result highlights that LSWI was highly sensitive to summer rainfall and the DNLSWI

rapidly decreased as the amount of rainfall increased. Specifically, the DNLSWI was more than 50 days when summer rainfall was less than 150 mm, indicating water stress (LSWI <0) during active growing period of the vegetation. Conversely, the DNLSWI was less than 2 weeks when summer rainfall was greater than 400 mm.

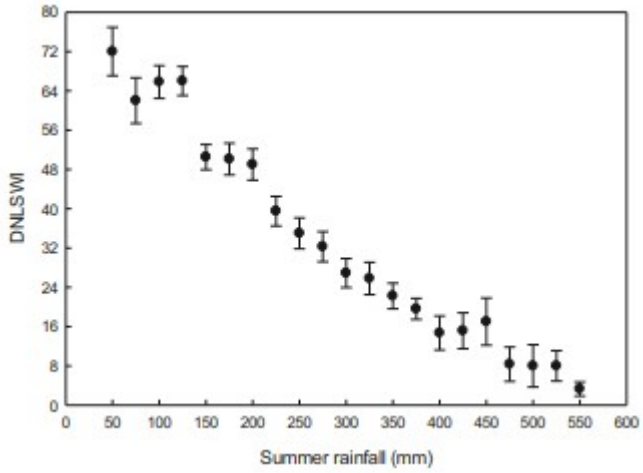

FIGURE 7 Relationship between summer rainfall and duration of LSWI <0. Each point is an average for all Mesonet stations binned by 50 mm of summer rainfall

The longitudinal gradient of summer rainfall is a widely recognized pattern in Oklahoma, where the amount of rainfall decreases from east (mean summer rainfall ~300 mm) to west (mean summer rainfall ~150 mm; Fig. 8a). To understand the occurrence of drought across the rainfall gradient of Oklahoma, we counted total DNLSWI during summer months (June–August) from 2000 to 2013 for all Oklahoma Mesonet stations. As expected, a distinct increasing pattern of total number of DNLSWI was observed across east-west gradient of Oklahoma (Fig. 8b), which was opposite to the rainfall pattern. The sites towards the east with greater amount of average summer rainfall had the least DNLSWI, whereas a general increment of DNLSWI was observed with lesser precipitation as we moved from east to west.

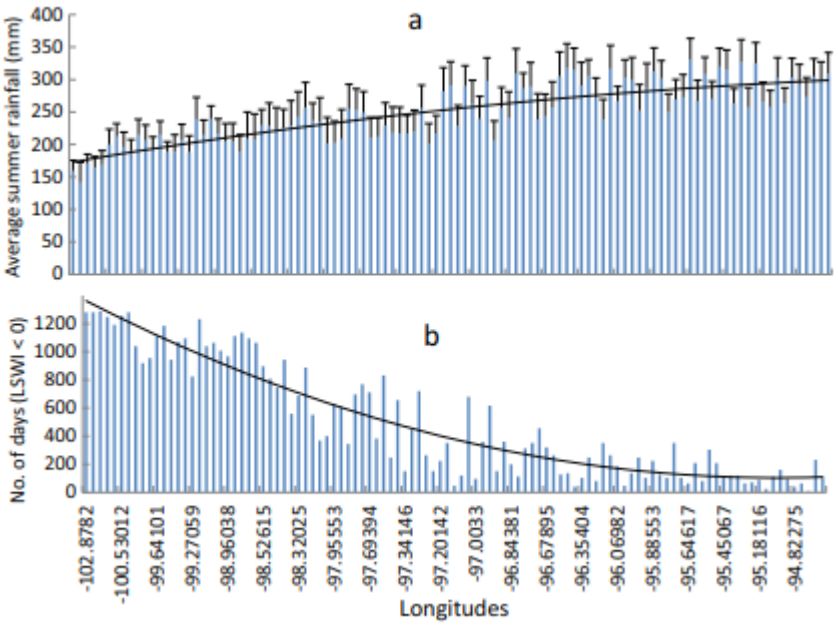

FIGURE 8 The performance of LSWI to track east-west rainfall gradient of Oklahoma: a average summer rainfall gradient from east to west and b DNLSWI (total number of days with LSWI <0 during summer months) from 2000 to 2013 for 113 Mesonet stations arranged by east-west geographical locations

Characteristics of DNLSWI and USDM drought history (2000–2013)

The pattern associated with DNLSWI for 113 Mesonet stations during the study period (2000–2013) is presented as box plots in Fig. 9a. These plots revealed the distribution of DNLSWI among the Mesonet sites within a year and among years. The median DNLSWI was relatively greater during the drought years (2000 = 32 days, 2006 = 48 days, 2011 = 56 days, and 2012 = 56 days) than non-drought years. The distribution as well as the median DNLSWI was the lowest in 2007, which was a pluvial year and the wettest summer on record in central Oklahoma (Arndt et al. 2009; Christian et al. 2015; Dong et al. 2011). Figure 9b shows the frequency distribution of the Mesonet stations (113 stations over 14 years) with associated DNLSWI (113 stations over 3 months) for the total study period and drought years separately. The count was highest for DNLSWI equal to 8 days because it is very common that majority of the stations could have LSWI below zero for 8 days over limited period during seasonal drying. However, the ratio of drought years to all years increased as the DNLSWI increased, suggesting that drought years contributed larger counts for the higher DNLSWI (Fig. 9c). For example, ratio of 0.13 for DNLSWI equal to 8 days means only 13 % of the total counts were contributed by the drought years, while for DNLSWI equal to 64 days, drought years contributed 63 % of the total counts, suggesting higher DNLSWI during the drought years.

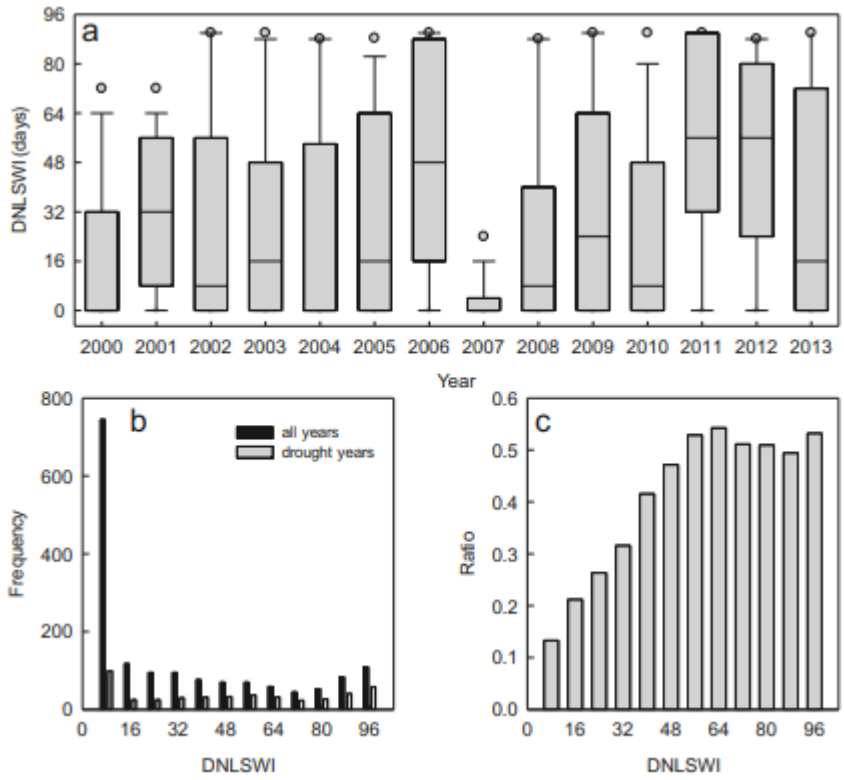

FIGURE 9 Duration of LSWI <0 (DNLSWI) across 113 Mesonet sites during 2000–2013 (a). The *solid lines in the box* represent the median, and the *dots above and below the box* represent the 95th and 5th percentiles, respectively. The frequency distribution of the Mesonet stations (113 stations × 14 years) with associated DNLSWI for 2000–2013 (b) and the ratio of number of stations with drought years to total years (drought and normal) for respective DNLSWI bins (c)

Figure 10 shows the weekly percentage of Oklahoma Mesonet sites affected by D_0 to D_4 drought from 2000 to 2013. The drought periods spanning 2006, 2011, and 2012 were evident and reached D_4 status for extended periods. The plot also depicts the pluvial condition during 2007 when D_0 drought occurred in a very limited temporal window. However, significant areas, especially sites in western Oklahoma where drought conditions persisted even though majority of the state yielded above normal precipitation, showed higher-intensity summer drought in 2013, which was also considered as an overall pluvial year based on total year rainfall.

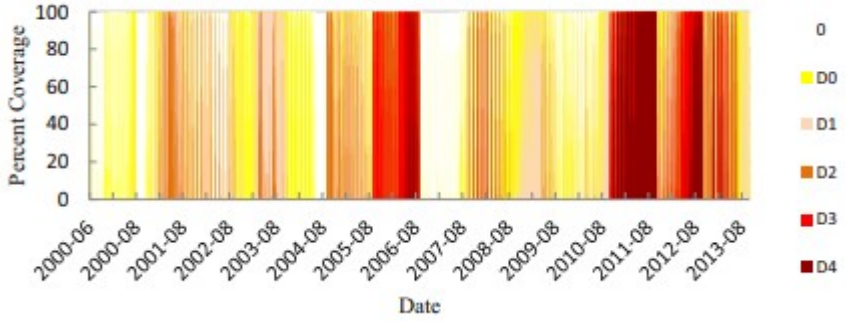

FIGURE 10 Percent of Oklahoma area covered by a USDM drought designation from 2000 to 2013. The designations 0 (no drought), D_0 (abnormally dry), D_1 (moderate drought), D_2 (severe drought), D 3 (extreme drought), and D_4 (exceptional drought) are the drought intensity classes defined by USDM (data source: US Drought Monitor)

The relationship between LSWI-based drought severity and USDM drought intensity categories

The LSWI values corresponding to its NDVI values for each week based on USDM weekly map are plotted in Fig. 11. Results showed that larger negative values of LSWI corresponded to higher drought intensity categories identified by USDM classes (i.e., D_3 and D_4—extreme and exceptional), while no drought and abnormally dry categories (0 and D_0) corresponded to the larger positive LSWI values. Further, moderate to severe drought categories (D_1 and D_2) corresponded to intermediate LSWI values. Based on this LSWI-NDVI two-dimensional scatter plot, we identified the range of LSWI values for each drought categories used by USDM in Bajgain et al. 2015. Due to the large number of site years and mixture of land cover types, the groupings of drought intensity could not be visualized effectively within the range formulated on observations at two tallgrass prairie sites. However, the general pattern that higher drought intensity tends to have lower LSWI values and vice versa was observed for all land cover types as well as grasslands and croplands. Compared to all land cover types and croplands, grasslands showed better relationships to the drought intensity categories.

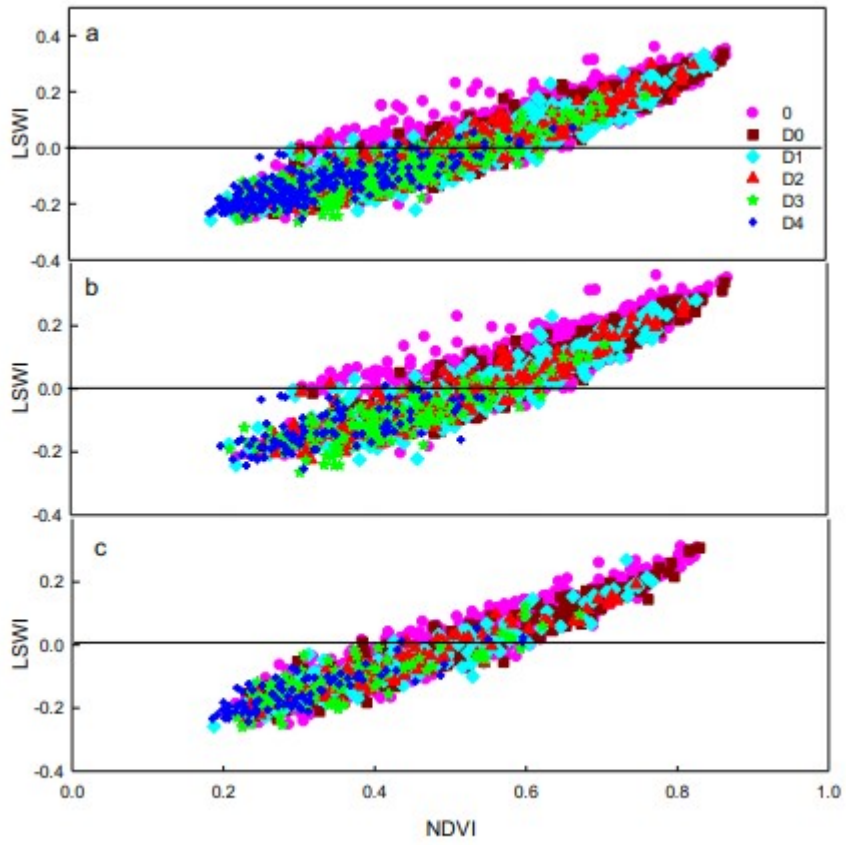

FIGURE 11 Relationship between NDVI and LSWI for individual pixels of the all types (a), grasslands (b), and croplands (c) of land cover sites for June–August over a 14-year study period (2000–2013). Each *point* in the plot represents the weekly observation of drought intensity designation for the study area as determined from US Drought Monitor (USDM) drought maps (http://droughtmonitor.unl.edu/MapsAndData/)

To determine the agreement between LSWI-based drought intensity classification based on the LSWI value range and USDM drought categories (Table 1), we computed the percentage of pixels that fall within the defined LSWI value range for the particular drought class. The assessment was performed for different land cover types (all land covers, grasslands, and croplands; Fig. 12a). Overall, the agreement was higher (>60 %) for low-intensity (0 and D_0) and high-intensity (D_3 and D_4) droughts (the two ends of drought class), but the intermediate drought intensity (D_1 and D_2) had relatively low agreement. However, the relationship was slightly improved when computed for individual land cover types with grasslands showing the best agreement. Furthermore, we analyzed the agreement of the LSWI-based drought classification for nine climate divisions of Oklahoma to further analyze the spatial variability of drought tracking by the LSWI-based algorithm (Fig. 12b). The LSWI identification showed better agreement (>80 %) with USDM 0 and D_0 (no dry and abnormally dry) classes in the eastern humid areas, whereas the agreement was low (<30 %) for the same drought classes in the western arid areas (panhandle). However, the western region

identified as severe to exceptional drought (D_3 and D_4) by USDM matched very well with the new LSWI-based classification. For example, 91 % of the pixels were classified as severe and exceptional droughts in the panhandle region, whereas USDM also identified the same drought intensity. However, only 19 % of the low-intensity drought pixels matched well with the lower-intensity drought classification of USDM.

Table 1 A summary of the USDM drought intensity classes and the LSWI-based classes

USDM drought intensity class	Description	LSWI *D* values
0	non-drought	LSWI > 0.1
D_0	abnormally dry	LSWI > 0.1
D_1	drought-moderate	0 < LSWI ≤ 0.1
D_2	drought-severe	−0.1 < LSWI ≤ 0
D_3	drought-extreme	LSWI ≤ −0.1
D_4	drought-exceptional	LSWI ≤ −0.1

Source: Bajgain et al. (2015)

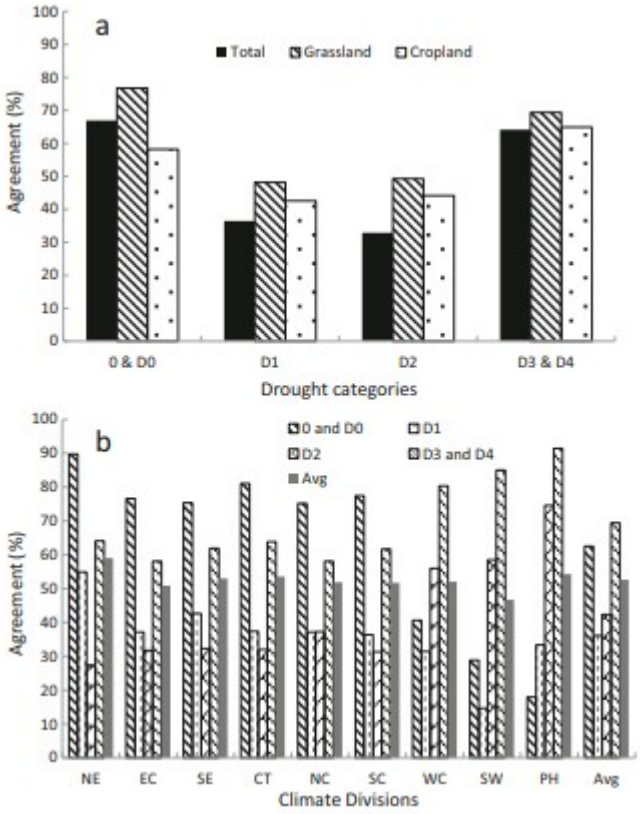

FIGURE 12 Agreement of the drought intensity class to the LSWI-based classification adapted from Bajgain et al. (2015) for different (a) land cover and (b) climate divisions of Oklahoma (*NE* northeastern, *EC* east central, *SE* southeastern, *CT* central, *NC* north central, *SC* south central, *WC* west central, *SW* southwestern, and *PH* panhandle)

The relationship between USDM drought intensity, DNLSWI, and average LSWI value is presented in Fig. 13. The general observation was that

drought intensity increased as DNLSWI became longer. For short DNLSWI periods (0–24 days), the drought impact was sharp and then plateaued between 24 and 48 days. As DNLSWI became larger (>48 days), the addition of each new day resulted into larger drought impacts identified as a higher drought intensity class by the USDM (Fig. 13). This relationship was further supported by the average LSWI values which declined as DNLSWI increased. The decreasing pattern of average LSWI was also persistent for the shorter DNLSWI but declined sharply as the DNLSWI was longer than 50–60 days.

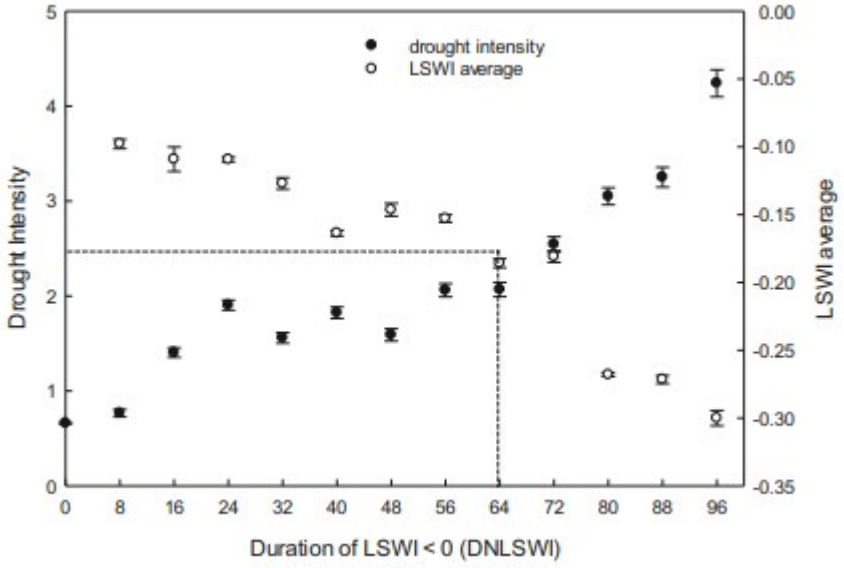

FIGURE 13 Relationship between USDM-based drought intensity classes, DNLSWI (duration of LSWI <0) and average LSWI. The USDM drought intensity classes 0, D_0, D_1, D_2, D_3, and D_4 are set to 0, 1, 2, 3, 4, and 5, respectively

Discussion

The correlation analyses between summer rainfall anomalies and LSWI anomalies in drought years revealed sensitivity of LSWI to summer rainfall variability in Oklahoma. Higher negative anomalies in summer rainfall resulted in larger decline in LSWI values, an indication of drought-impacted vegetation (Bajgain et al. 2015; Wagle et al. 2014). Regardless of different land cover and soil types across 113 Oklahoma Mesonet sites, LSWI tracked droughts in majority of the study sites. However, it over-classified the low-intensity droughts in arid western regions of Oklahoma. Given the anticipated future increase in precipitation variability (Liu et al. 2012; Zhang and Nearing 2005), ecosystems in this region are expected to be particularly susceptible to droughts resulting large losses for food and livestock industries. Our results suggested that the ability of LSWI to track the summer rainfall anomalies could be one of the important features to assess and track agricultural droughts. Our finding on the performance of LSWI to track water content of the ecosystem was consistent with the results by Chandrasekara

et al. 2011, which demonstrated LSWI as a potential indicator of increasing water content in the ecosystem following the onset of monsoon in India. Since commonly used NDVI and EVI are not always good indicators of vegetation conditions especially during adverse climatic conditions for vegetation growth (Gamon et al. 1995; Gamon et al. 1993), LSWI can better track the drought-impacted vegetation because of its higher sensitivity to drought (Bajgain et al. 2015; Chandrasekara et al. 2011; Tian et al. 2013; Wagle et al. 2014). The opposite longitudinal patterns of DNLSWI and summer rainfall suggested that counting the DNLSWI (in days) has the ability in tracking the drought across various Mesonet sites of Oklahoma. The results illustrate that LSWI can be used as an effective tool to monitor dryness persisted in the diverse (land cover and soil types) ecosystems in semi-arid and semi-humid regions in eastern and central Oklahoma. However, the spatial variability of drought tracking ability was observed based on drought intensity. In eastern humid regions of Oklahoma, both USDM-D and LSWI-D showed no drought (0 drought class) when average summer rainfall was above 250–300 mm (Table 2). However, in western dry region of Oklahoma, USDM- and LSWI-based drought categories were different. For example, above 150 mm of summer rainfall was considered as no drought categories by USDM, but LSWI showed severe drought category (D_3) with 150–300 mm of summer rainfall. The less agreement between our LSWI-based and USDM drought categories for the low drought intensity categories is because of the fact that dry areas like panhandle region of Oklahoma has higher negative LSWI values, and consequently, the LSWI-based algorithm showed higher drought severity. LSWI values are considered proxy of vegetation water content and are the physical values, whereas USDM considered several factors including local reports of drought conditions (such as reports from water managers and residents) (Svoboda et al. 2002). This made USDM assessment more locally adjusted despite of coarse spatial resolution.

Table 2 USDM- and LSWI-based drought classes in eastern and western Oklahoma binned by average summer rainfall of the Mesonet stations located in the areas

Summer rain (mm)	Eastern OK		Western OK	
	USDM *D* class	LSWI *D* class	USDM *D* class	LSWI *D* class
50–100	3	2	5	5
100–150	2	2	4	5
150–200	2	3	1	3
200–250	0.5	0.5	0	3.5
250–300	0	0	0.2	3
300–350	0	0	0	1.5
350–400	0	0	0	0
400–450	0	0		
450 above	0	0		

One of the main reasons behind attempting to establish the relationship between summer rainfall and LSWI was to determine the hydrological status of the ecosystem. The total amount of summer rainfall received by a

particular ecosystem in a particular year could be related to DNLSWI, which in turn can be inferred in terms of drought intensity. Although our results showed a smooth decreasing trend of DNLSWI with increasing summer rainfall, site-specific relationship could not be established (Bajgain et al. 2015) because averaging multiple data points produced a smoother overall trend. Thus, additional experiments are needed to identify the threshold values for each site with different soil and crop types in the future. Rainfall expressed as a percentage departure from the long-term average for a given period is widely used index for drought monitoring, where monitoring other parameters such as soil moisture or evapotranspiration are costly and difficult (Nicholson 1989; Nicholson 2000). With this approach, where total summer rainfall is inferred in terms of DNLSWI for assessing drought is extremely valuable since LSWI is derived from satellite sensors. Therefore, it is very important to apply this information rendered from LSWI and summer rainfall relationship while developing drought-monitoring network for this region.

Knowledge of LSWI-based drought intensity could be critical for assessing drought with different parameters like DNLSWI. Quantifying drought intensity in terms of LSWI and defining a threshold for each USDM drought class will be an important implication for a future drought-monitoring program. For example, secretarial disaster area determination and notification process depends on the USDM drought intensity classification for designating any geographical unit as a disaster area (USDA-FASA, 2015). The criteria used are the area should be under either D_3 or D_2 (at least 8 consecutive weeks) drought class. USDM drought classification involves a series of information for finding a threshold, comprised of complex procedures as well as could have a limited spatial precision because it relies on spatially interpolated climate data input (Tadesse et al. 2015). Our results suggested that this USDM drought intensity class can be linked with DNLSWI. The intersection of intensity curve and $LSWI_{avg}$ curves in Fig. 13 established a threshold point at which drought impacts increased sharply as $LSWI_{avg}$ declined. This threshold value is between the D_2 and D_3 drought intensity classes and can be inferred in terms of DNLSWI, which is approximately 60–62 days. Many agencies have used USDM drought intensity class thresholds to guide measures in a variety of assistance programs such as Livestock Forage Disaster Program (LFP), Emergency Haying and Grazing, Livestock Indemnity Program, Noninsured Crop Disaster Assistance Program (NAP), and Crop Insurance Basics (Mallya et al. 2013; Mizzell and Lakshmi 2003; Otkin et al. 2015). Such assistance programs can alternatively input DNLSWI thresholds for simple and easy operations as well as for a better precision in terms of spatial resolution (500 m). However, validation of this approach of LSWI-based thresholds for such kind of applications remains a further research topic.

The MODIS-derived, LSWI-based drought assessment algorithm is simple and has a higher spatial resolution (~500). However, the LSWI-based drought

algorithm can have a limitation when the reflectance from land surface is impacted by cloud cover (Jensen 2009). An appropriate gap-filling algorithm can create a continuous dataset, thereby reducing the effect of unreliable observations, which is needed for making the drought-monitoring algorithm robust. Another limitation is the threshold values used in the algorithm. We used LSWI <0 during the growing season as the indicator of agricultural drought in tallgrass prairie based on calibration made on two study sites (Bajgain et al. 2015). Although the algorithm showed good agreement in most of the Mesonet sites, the DNLSWI clearly over-classified D_0 and D_1 drought conditions in the arid regions of Oklahoma. This is because these regions receive less rainfall than the semi-arid to semi-humid regions of eastern Oklahoma, where the algorithm was originally calibrated. This result suggests that it is necessary to further refine the LSWI-based algorithm to better represent drought severity in arid western regions of Oklahoma. One of the possible adjustments could be the LSWI threshold values for the arid region considering more negative magnitudes of the LSWI values in arid regions. This adjustment could reduce the discrepancies observed between the LSWI and USDM drought classification especially for lower drought intensity resulted from the larger negative values of LSWI, a common feature of arid region.

Conclusions

Results of LSWI analysis for the period of 2000–2013 for 113 Mesonet stations across Oklahoma revealed valuable information within the context of drought tracking. A strong correlation and dynamics between LSWI anomalies and summer rainfall anomalies comprises a fact that LSWI is sensitive to rainfall variations and can be used as an indicator of drought occurrence in an ecosystem. It is then deduced that DNLSWI had the close association with the vegetation condition under rainfall variations. Pixel-based drought intensity classification has been tested to validate the LSWI-based drought class for different land cover and soil types. Despite a relatively lower degree of agreement for the intermediate drought classes, the LSWI-based drought intensity class was reliable for low- and high-intensity classes defined by USDM. There was a longitudinal sensitivity for low-intensity droughts between eastern and western Oklahoma as shown by lower agreement of D_0 and D_1 drought with USDM in panhandle region (western Oklahoma). The drought assessment at larger scale could be made more effective by incorporating information and features of LSWI such as DNLSWI from a site level to a regional scale with further improvement for arid regions, where larger negative LSWI values are common. The analogy of DNLSWI to USDM drought intensity class could be made complement in current drought-monitoring program and algorithms. Results also demonstrated that by counting the number of DNLSWI, drought intensity thresholds can be established and used as a simple complementary tool in several applications.

Acknowledgments

This study was supported in part by a research grant (Project No. 2012-02355) through the USDA National Institute for Food and Agriculture (NIFA)'s Agriculture and Food Research Initiative (AFRI), Regional Approached for Adaptation and Mitigation of Climate Variability and Change grant (IIA-1301789), NOAA Climate Office's Sectoral Applications Research Program (SRP) grant NA130AR4310122, and Oklahoma's taxpayers fund for the Oklahoma Mesonet through the Oklahoma State Regents for Higher Education and the Oklahoma Department of Public Safety. We would also like to acknowledge the National Drought Mitigation Center at the University of Nebraska-Lincoln, the US Department of Agriculture, and the National Oceanic and Atmospheric Administration for the dataset.

References

Arndt DS, Basara JB, McPherson RA, Illston BG, McManus GD, Demko DB (2009) Observations of the overland reintensification of tropical storm Erin (2007). Bull Am Meteorol Soc 90:1079–1093

Bajgain R, Xiao X, Wagle P, Basara J, Zhou Y (2015) Sensitivity analysis of vegetation indices to drought over two tallgrass prairie sites. ISPRS J Photogramm Remote Sens 108:151–160

Basara JB, Maybourn JN, Peirano CM, Tate JE, Brown PJ, Hoey JD, Smith BR (2013) Drought and associated impacts in the Great Plains of the United States—a review. Int J Geosci 4:72

Brock FV, Crawford KC, Elliott RL, Cuperus GW, Stadler SJ, Johnson HL, Eilts MD (1995) The Oklahoma Mesonet: a technical overview. J Atmos Ocean Technol 12:5–19

Ceccato P, Flasse S, Gregoire J-M (2002) Designing a spectral index to estimate vegetation water content from remote sensing data: part 2. Validation and applications. Remote Sens Environ 82:198–207

Ceccato P, Flasse S, Tarantola S, Jacquemoud S, Grégoire J-M (2001) Detecting vegetation leaf water content using reflectance in the optical domain. Remote Sens Environ 77:22–33

Chandrasekara K, Saia MS, Beheraa G (2011) Assessment of early season agricultural drought through land surface water index (LSWI) and soil water balance model. ISPRS-International Archives of the Photogrammetry, Remote Sensing and Spatial Information Sciences 3820:50–55

Christian J, Christian K, Basara JB (2015) Drought and pluvial dipole events within the great plains of the United States. J Appl Meteorol Climatol 54:1886–1898

Dong X et al. (2011) Investigation of the 2006 drought and 2007 flood extremes at the Southern Great Plains through an integrative analysis of observations. J Geophys Res Atmos 116(D3). doi: 10.1029/2010JD014776

Gamon JA et al. (1995) Relationships between NDVI, canopy structure, and photosynthesis in three Californian vegetation types. Ecol Appl:28–41

Gamon JA, Field CB, Roberts DA, Ustin SL, Valentini R (1993) Functional patterns in an annual grassland during an AVIRIS overflight. Remote Sens Environ 44:239–253

Hoerling M et al. (2013) Anatomy of an extreme event. J Clim 26:2811–2832

Hulse JH, Escott VJ (1986) Drought–inevitable and unpredictable the pattern and consequences of recurrent drought interdisciplinary. Science Reviews 11:346–358

Hunt ER, Rock BN, Nobel PS (1987) Measurement of leaf relative water content by infrared reflectance. Remote Sens Environ 22:429–435

Jackson R, Slater P, Pinter P (1983) Discrimination of growth and water stress in wheat by various vegetation indices through clear and turbid atmospheres. Remote Sens Environ 13:187–208

Jensen JR (2009) Remote sensing of the environment: an Earth resource perspective. Pearson Education, New Delhi

Kogan F (2002) World droughts in the new millennium from AVHRR-based vegetation health indices. Eos Transactions American Geophysical Union 83:557–563

Kogan F, Stark R, Gitelson A, Jargalsaikhan L, Dugrajav C, Tsooj S (2004) Derivation of pasture biomass in Mongolia from AVHRR-based vegetation health indices international. Journal of Remote Sensing 25:2889–2896

Lillesand T, Kiefer RW, Chipman J (2014) Remote sensing and image interpretation. Wiley, New York

Liu L, Hong Y, Bednarczyk CN, Yong B, Shafer MA, Riley R, Hocker JE (2012) Hydro-climatological drought analyses and projections using meteorological and hydrological drought indices: a case study in Blue River basin. Oklahoma Water Resources Management 26:2761–2779

Maki M, Ishiahra M, Tamura M (2004) Estimation of leaf water status to monitor the risk of forest fires by using remotely sensed data. Remote Sens Environ 90:441–450

Mallya G, Zhao L, Song X, Niyogi D, Govindaraju R (2013) 2012 Midwest drought in the United States. J Hydrol Eng 18:737–745

Mizzell HP, Lakshmi V (2003) Integration of science and policy during the evolution of South Carolina’s drought program water: science, policy, and management: challenges and opportunities 311–339

Nicholson SE (1989) Long-term changes in African rainfall. Weather 44:46–56

Nicholson SE (2000) The nature of rainfall variability over Africa on time scales of decades to millenia. Glob Planet Chang 26:137–158

Otkin JA, Shafer M, Svoboda M, Wardlow B, Anderson MC, Hain C, Basara J (2015) Facilitating the use of drought early warning information through interactions with agricultural stakeholders. Bull Am Meteorol Soc 96:1073–1078

Shahid S, Behrawan H (2008) Drought risk assessment in the western part of Bangladesh. Nat Hazards 46:391–413

Sönmez FK, Koemuescue AU, Erkan A, Turgu E (2005) An analysis of spatial and temporal dimension of drought vulnerability in Turkey using the standardized precipitation index. Nat Hazards 35:243–264

Svoboda M et al. (2002) The drought monitor. Bull Am Meteorol Soc 83:1181–1190

Tadesse T, Wardlow BD, Brown JF, Svoboda MD, Hayes MJ, Fuchs B, Gutzmer D (2015) Assessing the vegetation condition impacts of the 2011 drought across the US southern Great Plains using the vegetation drought response index (VegDRI). J Appl Meteorol Climatol 54:153–169

Tian Y, Zhou L, Romanov P, Yu B, Ek M 2013 Comparison of Amazon and central Africa tropical vegetation dynamics using SEVIRI data from 2009 to 2011. In: EGU General Assembly Conference Abstracts. p 6535

United States Department of agriculture farm service agency (USDA-FSA) (2015) Noninsured crop cisaster assistance program (NAP). http://www.fsa.usda.gov/Internet/FSA_File/ccc0471_nap_bp_140813v01.pdf. Acessed July 2016

Wagle P et al. (2014) Sensitivity of vegetation indices and gross primary production of tallgrass prairie to severe drought. Remote Sens Environ 152:1–14

Zhang X, Nearing M (2005) Impact of climate change on soil erosion, runoff, and wheat productivity in central Oklahoma. Catena 61:185–195